
Article:
Hooley, R orcid.org/0000-0002-3515-4195, Brown, A orcid.org/0000-0001-9692-2154 and Drummond-Brydson, R orcid.org/0000-0003-2003-7612 (2019) Factors affecting electron beam damage in calcite nanoparticles. Micron, 120. pp. 25-34. ISSN 0968-4328

https://doi.org/10.1016/j.micron.2019.01.011

Factors affecting electron beam damage in calcite nanoparticles

Rob Hooley [a*], Andy Brown [a+], Rik Brydson [a#]
a - School of Chemical and Process Engineering, University of Leeds, Leeds, LS2 9JT, UK
* - pmrh@leeds.ac.uk (corresponding author)
+ - a.p.brown@leeds.ac.uk
# - r.m.drummond-brydson@leeds.ac.uk

Abstract

We report electron fluence thresholds for the degradation of calcite nanoparticles under electron irradiation by both conventional and scanning TEM (CTEM and STEM), using time resolved phase contrast imaging and EDX spectroscopy at both 80 kV and 300 kV accelerating voltages. We show that the degradation pathway of calcite involves disruption of the crystal lattice with the evolution of pores and transformation to calcium oxide and carbon dioxide. Depending on irradiation conditions (CTEM or STEM), the calcium oxide formed can be either amorphous or crystalline, with the formation of the latter apparently being hindered by hydrocarbon contamination build up in STEM. For a given electron flux, irradiation at 300 kV prolongs the characteristic lifetime of the calcite lattice as compared to irradiation at 80 kV but with a corresponding reduction in both image contrast and energy dispersive X-ray (EDX) signal, consistent with the change in inelastic mean free path for electron scattering. STEM offers significant benefits over CTEM, however only in the presence of hydrocarbon contamination, increasing the fluence threshold for the detection of irradiation induced faults in the calcite lattice from 2.7×10^{7} $e^{-}nm^{-2}$ for 300 kV CTEM to over 1.8×10^{8} $e^{-}nm^{-2}$ for 300 kV STEM. This work forms a framework for reliable identification of discrete particle crystallinity in nominally amorphous, nanoscale calcium carbonate particles which is of importance for fundamental studies of crystallisation and also for the process control during the synthesis of such surfactant stabilised nanoparticles for application as over-based fuel detergents.

Keywords

Electron beam damage
Phase contrast

Calcium carbonate
STEM
Hydrocarbon contamination

1 Introduction

Calcium carbonate is of widespread interest as a structural biomaterial and for its environmental and industrial importance. It is an important model system for fundamental studies of nucleation, growth and polymorphism in inorganic crystals (Nielsen et al., 2012). Biologically, calcium carbonate is often found in structural composites typically embedded in a biological polymer matrix, an example of this being iridescent nacre in mollusc shells (Rae Cho et al., 2016). In an industrial context, calcium carbonate is found as both a filler and as an active ingredient in formulated products, for example, nanoscale calcium carbonate particles stabilised by a surfactant are used in over-based fuel detergents to neutralise acid build-up in combustion engines (Mansot et al., 1993; Srot et al., 2013).

Analytical electron microscopy is an important tool for studying structure and chemistry at sub-nanometre resolution. However, calcium carbonate is known for its sensitivity to electron irradiation in both conventional and scanning transmission electron microscopy (CTEM and STEM respectively); the damage process and its onset having been semi-quantitatively discussed in recent reports (Golla-Schindler et al., 2014; Hoffmann et al., 2014; Hooley et al., 2017; Kovarik et al., 2016; Murooka and Walls, 1991; Walls and Tence, 1989). Under both CTEM and STEM irradiation, crystalline calcium carbonate is known to degrade into crystalline calcium oxide, with the loss of carbon dioxide and it has been suggested that the degradation proceeds via an amorphous intermediate compound of either calcium carbonate or calcium oxide, from which the oxide crystallises (Golla-Schindler et al., 2014). Amorphous calcium carbonate has been shown to form crystalline calcium oxide as a damage product under electron irradiation, impacting on the study of materials of unknown or mixed crystallinity (Jacob et al., 2011; Rodriguez-Navarro et al., 2016). For example, there is an ongoing debate as to the extent of crystallinity and the crystal structures present in the core of the over-based fuel detergent nanoparticles discussed above (Hudson et al., 2006). In this

case, separating the identification of pristine crystallinity from beam induced crystallinity requires a much more fundamental and quantitative understanding of how damage progresses. By quantifying the onset of the different stages of degradation that calcium carbonate undergoes during electron beam induced decomposition, it is possible to derive “safe” thresholds for electron fluence, electron flux and ultimately electron dose. These thresholds can provide confidence that CTEM/STEM images as well as EELS and EDX spectra of calcium carbonate are representative of its pristine state and reliable conclusions can be inferred from analytical microscopy data of crystallinity, polymorphism, defects and surface structure in this material.

Electron beam damage is a complex problem arising from a combination of multiple competing mechanisms. Separating the influence of each mechanism is often challenging, although the dominant damage mechanism can be inferred by adjusting the operating conditions of the microscope and observing the effect on the material under investigation. Calcium carbonate is an insulator and is commonly believed to degrade under electron irradiation by radiolytic fission of the carbonate group, forming calcium oxide and carbon dioxide, however its susceptibility to other forms of electron beam damage is not well understood. Rodriguez-Navarro et al., (2009) state that the type of energy used to transform $CaCO_3$ to CaO does not affect the decomposition mechanism (i.e. either electron irradiation or thermal heating). They also propose three stages for the decomposition of $CaCO_3$: energy transfer to the reaction interface (via excitation of electrons into the conduction band), fission of the O-C bond to produce CaO and CO_2 (via de-excitation of the excited electrons to the ground state), and diffusion of CO_2 through the product layer. They believe that the rate limiting step is the fission of the O-C bond, and that the diffusion of CO_2 is not rate limiting due to the presence of pores and voids induced by the volume change of $CaCO_3$ to CaO facilitating its egress to vacuum or air. Since the damage process is not diffusion limited nor is a healing reaction possible due to the irreversible loss of CO_2 and given our prior report that shows critical fluences for visible damage phenomena are independent of electron flux we suggest that the electron beam damage of calcite is a linear process, i.e. the damage rate displays no

electron flux dependence (Hooley et al., 2017). Hills, (1968) states that decomposition occurs at the boundary between unreacted calcium carbonate and porous calcium oxide, which then progresses into the core of the particle from the outer edges. Cazaux, (1995) also states that radiolysis progresses from particle surfaces towards the core in part because electrons associated with surface atoms, at defect sites or at grain boundaries are less strongly bound and are thus more susceptible to radiolysis; this is in part why thick specimens damage more slowly than thinner specimens of the same composition.

Previous research by Kabalah-Amitai et al., (2013) claimed that operating the microscope at 80 kV rather than 300 kV in CTEM was beneficial for high resolution imaging in calcium carbonate, presumably through an improvement in image contrast provided by increased elastic scattering, however accumulated doses, fluences or electron fluxes were not quantified. This is despite the general understanding that radiolytic damage rates drop with increasing kV because the cross section for inelastic scattering is inversely proportional to accelerating voltage (e.g. Egerton, 2012). In addition, the use of STEM may be beneficial, because the rastering motion of the focused probe may allow for heat and charge to dissipate, reducing damage from radiolysis and subsequent beam induced heating. The use of STEM also allows for more practical control of electron fluence as probe focussing and fine alignment can be performed on the support film immediately adjacent to a region of interest by using the Ronchigram from a stationary probe prior to scanning. Potentially this reduces the time the specimen spends under the beam.

The intentional deposition of conductive coatings has well known benefits for the reduction of charging in SEM sample preparation, as the coating provides an efficient pathway for the neutralisation of excess or depleted electrons as well as acting to inhibit sputtering induced mass-loss in CTEM and STEM (when the coating is applied to the specimen exit surface) (Egerton, 2013). Thus, it is pertinent to investigate whether hydrocarbon contamination build up on the surface of a specimen during STEM irradiation is effective as a means of extending the lifespan of calcium carbonate particles. Surface contamination in the STEM is attributed to the cracking and polymerisation of surface hydrocarbons, present on

specimens exposed to ambient conditions, residues from the production of carbon support films, and residues from vacuum oils and greases in the microscope column (Hirsch et al., 1994). Using 200 kV STEM on the sheet silicate mineral biotite, Ward et al., (2013) have demonstrated an electron fluence threshold for the transition from, electron beam induced contamination build up on the surface of biotite thin sections under the focussed probe to mass loss, or hole-drilling within the sections. Working below this fluence threshold they were able to obtain nanometre-scale structural (atomic lattice resolution by diffraction and phase contrast imaging) and elemental (EDX) information from biotite. In other previously published examples, the use of intentionally deposited coatings has been shown to reduce the susceptibility of radiation damage through several methods. Chen et al., (2010) have demonstrated the application of a platinum coating to reduce knock-on damage when irradiating sapphire specimens in CTEM. Smith, (1986) also demonstrated the impact of the addition of conductive coatings to the radiation sensitivity of calcite and dolomite in electron probe microanalysis at 15 kV. It was found that the addition of the conductive layers supressed damage by assisting in charge neutralisation, which reduced the impact of beam damage by a factor of 25 times, although this significantly reduced the X-ray counts measured.

The focus of the current research is to identify and quantify electron fluence thresholds for irradiation induced degradation of calcite nanoparticles during phase contrast CTEM and STEM imaging, selected area electron diffraction and energy dispersive X-ray spectroscopy at both 80 and 300 kV. Ultimately the study aims to determine the most beneficial operating conditions for application of analytical electron microscopy to the characterisation of calcium carbonate based nanomaterials.

2 Materials and Methods

2.1 Materials

Calcite nanoparticles of approximately 50 nm in diameter were produced in-house by the carbonation of calcium oxide suspended in deionised water using the method reported by Hari et al., (2006); briefly calcium oxide was prepared by the thermal decomposition of calcium

carbonate (AR grade, Fisher Scientific), heated to 900 ^{o}C for 5 hours. Production of a particular calcite polymorph was confirmed by Raman spectroscopy and X-ray diffraction (data not shown). The particles were air dried and then suspended in ≥99.5% ethanol (molecular biology grade, Fisher Scientific) prior to deposition onto either a holey carbon or lacy carbon film (Agar Scientific Ltd) for 200 kV experiments, and an ultrathin amorphous carbon (Agar Scientific Ltd) or graphene oxide film (EM Resolutions Ltd) for 300 kV and 80 kV experiments, all supported on copper TEM grids.

2.2 Initial qualitative CTEM irradiation study at 200 kV

CTEM irradiation experiments were carried out at 200 kV in a FEI Tecnai F-20 FEG-TEM with an Oxford Instruments X-Max 80 mm^2 EDX detector and a Gatan Orius CCD. Controlled irradiation at several electron fluxes was applied to the calcite nanoparticles, bright field (BF) mass-thickness contrast images and selected area diffraction patterns (SADPs; with a circa 200 nm diameter selected area aperture inserted at the image plane) were taken at fixed timed intervals. Prior to imaging and diffraction, the electron beam was blanked and the flux reduced to avoid unintended irradiation. The presence of polycrystalline calcium oxide in SADPs was investigated by analysing the CaO {111} and {200} diffraction rings. SADPs were processed using the “reveal weak reflections” tool in the Difftools plugin for Gatan Microscopy Suite 3.11 (Mitchell, 2008).

2.3 Comparing CTEM and STEM irradiation using time resolved phase contrast imaging

A comparative study of electron beam sensitivity in STEM and CTEM was performed in a FEI Titan^3 Themis G2. Phase contrast (PC) CTEM lattice images were taken at 80 kV and 300 kV with an electron flux of 3.8x10^5 e$^-$nm^{-2}s^{-1} at 380,000 times magnification on a Gatan OneView CCD. Phase contrast STEM images were taken at 300 kV with a probe current of 40 pA, 16 µs dwell time and a specimen pixel size of 57.8 pm giving an averaged fluence of 1.2x10^6 e$^-$ nm^{-2} per scan, calculated by the following equation.

$$Fluence(e^{-}nm^{-2}) = \frac{I \times t}{e^{-} \times d_s^2}$$

Where t is the dwell time, I is the probe current, e^- is the charge of an electron (1.602×10^{-19} C) and d_s is the pixel size

The probe convergence semi angle was 10 mrad, giving a 1.4 Å probe, the FEI bright field detector collection semi angle was set to circa 7 mrad at a camera length of 460 mm, providing phase contrast with the optimum collection efficiency for an uncorrected STEM (Sader et al., 2010). The FFTs of both CTEM and STEM images were compared to investigate changes in crystallinity induced by electron irradiation.

2.4 Comparing impact of accelerating voltage on mass loss using time resolved EDX spectroscopy

To compare the extent of mass loss in CTEM under irradiation at 80 kV and 300 kV, calcite nanoparticles were drop cast onto a lacy carbon film supported on a copper TEM grid. EDX measurements were taken on a FEI Titan^3 Themis G2 with a Super-X EDX system, operating at 300 kV and 80 kV in CTEM mode, using a FEI low background analytical double tilt sample holder. Consecutive spectra were taken for 80 and 300 kV measurements, with live times of 30 and 15 s respectively at an electron flux of 3.5×10^4 $e^- nm^{-2} s^{-1}$. The beam was blanked between acquisitions to avoid excess irradiation, accumulated fluences were calculated using the live spectrum acquisition duration and the measured probe current (based on the flu-cam current reading which had been calibrated by a Faraday cup).

Multiple spectra were acquired from a region of the carbon support close to the irradiated particles, using the same beam and spectrum acquisition conditions. These spectra were then averaged to produce a background spectrum for subtraction from the calcite plus support film spectra. This was done in order to reduce the impact of residual oxygen associated with the carbon support film on the quantification of oxygen in the calcite particles. Spectra were analysed using the DTSA-II software package (Ritchie, 2011), for background subtraction and peak integration of the Ca Kα and O Kα peaks. The EDX k-factor for quantification of the oxygen to calcium atomic ratio was calculated assuming that the first spectrum was representative of calcium carbonate stoichiometry i.e. a 3:1 ratio of oxygen to calcium.

To investigate X-ray count rates for 80 kV and 300 kV operation, isolated calcite nanoparticles were irradiated at a flux of 3.4×10^4 $e^- nm^{-2} s^{-1}$ for a total accumulated fluence of

10^6 e^-nm^{-2} (i.e. 30 s live time spectrum acquisition). This was repeated for multiple particles at both beam voltages, with the average Ca-Kα and O-Kα peak areas compared. For this study the spectral background was not subtracted.

2.5 In-situ sample bake-out

To reduce the impact of hydrocarbon contamination during STEM imaging, a calcite sample was drop cast from ethanol onto a silicon nitride MEMS heater grid (DENS Solutions) and loaded into the microscope in a DENS Solutions wildfire single tilt holder. The hydrocarbon contamination was quantified first with the sample unheated, by measuring the contamination growth perpendicular to particle facets after each scan, using ADF-STEM imaging at 320,000 times magnification,10 µs dwell time, 40 pA probe current and at a camera length of 460 mm, giving an ADF collection semi-angle range of 17-100 mrads. Measurements of contamination thickness were taken using line profiles in the Gatan Microscopy Suite software package, with a 5 pixel integration width. The sample was then heated to 75 ^oC and held for 16 hours before cooling to 25 ^oC over 1 hour. Following heat treatment, the contamination build-up was then quantified using the same method on a fresh region of the sample, to ensure contamination desorption. The specimen was then imaged using the same methods as outlined in section 2.3.

3 Results

3.1 Qualitative observations of electron beam damage in calcite

3.1.1 Manifestation of damage

As observed by low magnification, bright field CTEM imaging at 200 kV, the calcite nano-particles became visibly damaged under irradiation and pores/voids emerge throughout the projected images of each particle (Figure 1), typically of the order of 2-4 nm in diameter. Porosity and void formation were mentioned by Towe, (1978) in calcite undergoing irradiation, although the fluence for their appearance is not quantified. In both cases alteration appeared to progress from the outer edges of the particles towards the bulk. Pores were seen to first appear here at 1.9×10^6 $e^- nm^{-2}$, independent of electron flux (Hooley et al., 2017).

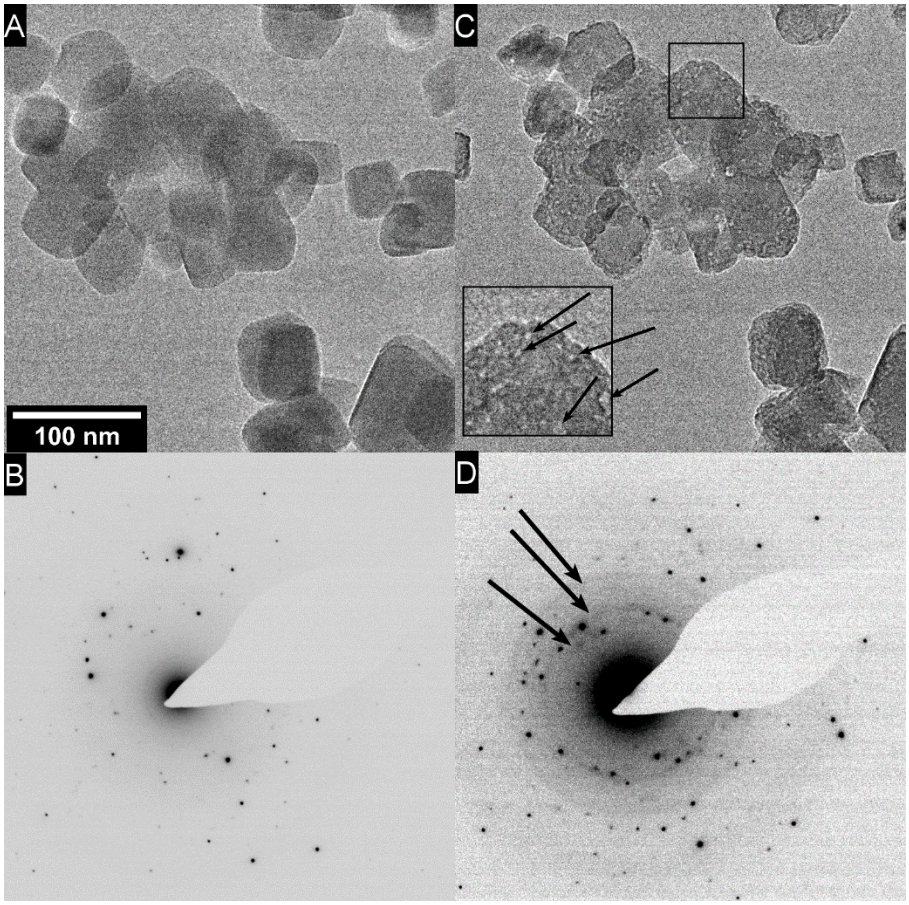

Figure 1 – 200 kV BF-CTEM images showing A) near pristine calcite nanoparticles and B) calcite only reflections in SADP of the pristine calcite images C) significant pore/void formation, pores indicated by arrows on the inset and D) the appearance of the calcium oxide {111} and {200} rings indicated by arrows (C and D following exposure to 3.8×10^6 $e^- nm^{-2}$ at 200 kV). 100 nm scale bar.

As the calcite was irradiated, calcium oxide rings appeared amongst the calcite spots. Time resolved electron diffraction showed the formation of polycrystalline calcium oxide was first detected after 3.9×10^6 $e^- nm^{-2}$ at 200 kV (Hooley et al., 2017). This was also noted by Towe,

(1978), Rodriguez-Navarro et al., (2009) and Hoffmann et al., (2014), where irradiated calcite showed both calcite diffraction spots, and calcium oxide diffraction rings concurrently, suggesting the progressive degradation of calcite.

EDX spectra taken at fluences ranging across the observed degradation of calcite particles under irradiation (i.e. pore formation in bright field imaging and CaO formation in SADPs) showed small, systematic reductions in the oxygen and carbon Kα peak areas with increasing fluence. No change was observed in the calcium Kα peak area. Reduction in oxygen and carbon is assumed to be due to the loss of carbon dioxide from the irradiated and altered calcite. In section 3.2 this change in peak area under irradiation was further investigated at higher fluences in order to assess the rate of mass loss at 80 kV and 300 kV.

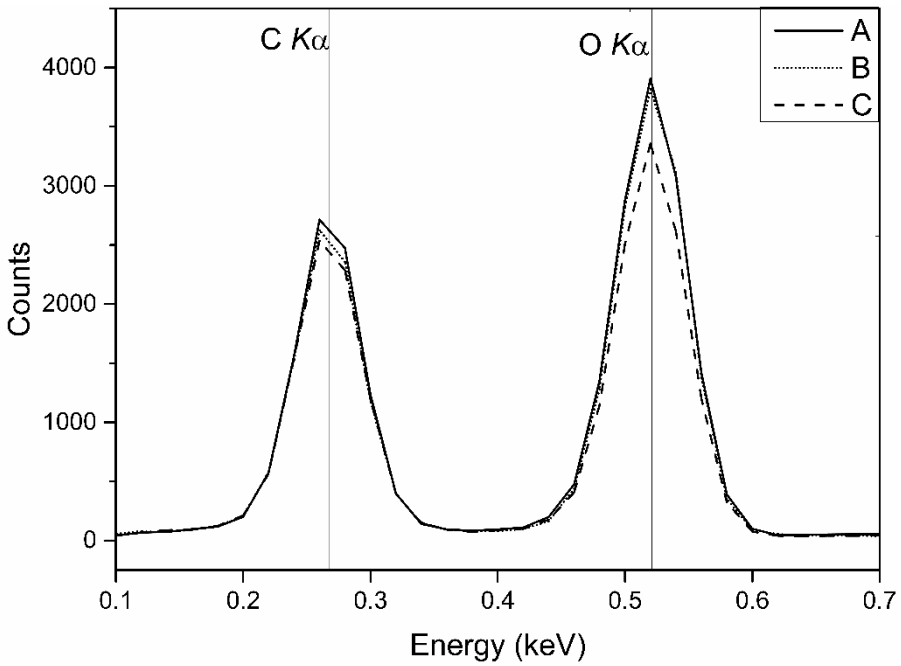

Figure 2 – CTEM EDX spectra of calcite particles under 200 kV irradiation after A) 8.2x10^{5} e^{-}nm^{-2} B) 1.7x10^{6} e^{-}nm^{-2}, close to the fluence at which pores became visible in bright field images (Figure 1C) and C) 4.1x10^{6} e^{-}nm^{-2}, close to the fluence at which polycrystalline CaO was detected in SADPs (Figure 1D).

3.2 Comparing CTEM irradiation at 80 and 300 kV

Under 300 kV CTEM irradiation the fast Fourier transform (FFT) of phase contrast (PC) CTEM images of the calcite nanoparticles began to show degradation of the calcite lattice, at an average fluence of 2.7x10^{7} e^{-}nm^{-2} with a standard deviation of ± 4x10^{6} e^{-}nm^{-2}, (Figure 3b; spots

in the FFT display some streaking/arcing at this fluence). This is not necessarily the nucleation of calcium oxide, but is the beginning of the breakdown of calcite crystallinity. Arcing of the FFT spots is caused by the disruption of the calcite lattice by the incident electrons, the atomic planes are distorted or bent over a short range with respect to the pristine lattice. This threshold is at a fluence just lower than that established for the onset of pore formation by bright field CTEM (Hooley et al., 2017). Pores/voids were directly visible in the particle irradiated at 2.9x10^{7} e^{-}nm^{-2} and are indicated by the arrows in Figure 3b.

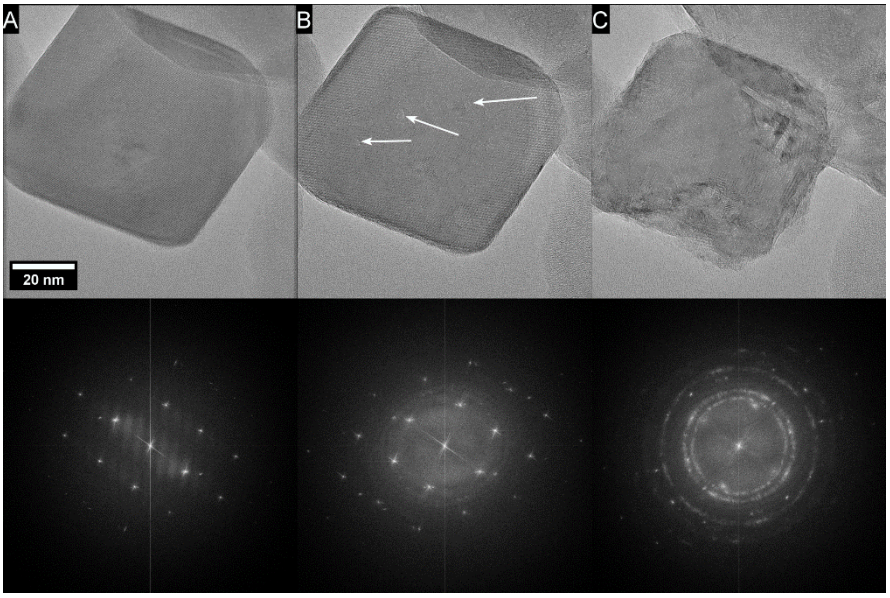

Figure 3. 300 kV phase contrast-CTEM images and FFTs (indicating the $[4\bar{4}1]$ zone axis orientation of a calcite nanoparticle) at accumulated fluences: A – 6.1x10^{6} e^{-}nm^{-2}, B – 2.9x10^{7} e^{-}nm^{-2} and C - 1.7x10^{8} e^{-}nm^{-2}. 20nm scale bar, arrows show pore formation in the calcite nanoparticle.

Under similar PC CTEM imaging conditions but at 80 kV, the lattice began to degrade on average at 1.7x10^{7} e^{-}nm^{-2} with a standard deviation of ± 2x10^{6} e^{-}nm^{-2} a lower average fluence when compared to 300 kV operation; this is shown in Figure 4b, where the spots show the same streaking/arcing that occurs at 300 kV (Figure 3b) was observed in the 80 kV FFT. Working at higher accelerating voltages is expected to extend the damage threshold for materials sensitive to radiolytic fission since there is an increase in inelastic mean free path length at higher accelerating voltages and therefore less energy would be deposited in the material at a given fluence (e.g. Egerton, 2014).

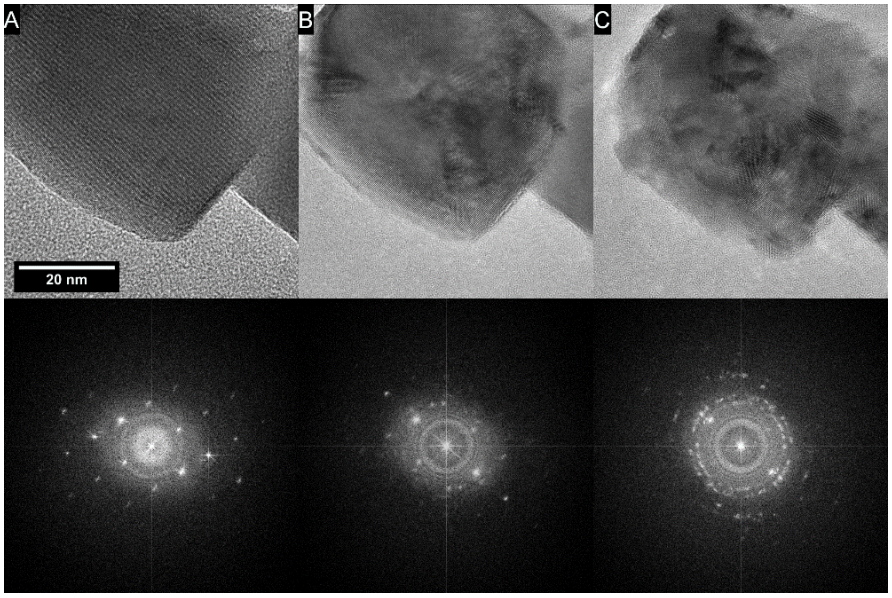

Figure 4. 80 kV PC-CTEM images and FFTs (indicating the $[\bar{6}00]$ zone axis orientation of a calcite nanoparticle) at accumulated fluences of A) 4.8x10^6 e$^-$nm^{-2} B) 1.7x10^7 e$^-$nm^{-2} and C) 4.7x10^7 e$^-$nm^{-2}. 20nm scale bar.

Whilst lattice resolution imaging provided insights into the degradation of calcite crystallinity, EDX spectroscopy can be used to investigate mass loss and its implications for compositional analysis. Any production and loss of carbon dioxide can be picked up by quantifying changes in oxygen and carbon Kα EDX peak areas. Any reduction in the calcium *Kα* peak area would suggest the additional presence of knock-on or sputtering damage occurring, likewise a continuing reduction in O:Ca ratio below 1:1 would indicate oxygen mass loss through sputtering. Calcium along with oxygen and carbon is likely to be more susceptible to knock-on damage above 80 kV (Egerton et al., 2004).

Changes in the O:Ca Kα peak area ratio of calcite nanoparticles irradiated at 80 kV and 300 kV in CTEM showed a clear reduction in oxygen peak area, interpreted as the removal of carbon dioxide by radiolysis (Figure 5). No change was detected in the calcium peak area up to 10^8 e$^-$nm^{-2}, suggesting that calcite is mostly susceptible to radiolysis at these fluences, as no calcium is removed through knock on or sputtering, even at 300 kV although this may not be the case at higher accelerating voltages or higher fluences.

At 80 or 300 kV, by 10^8 e$^-$nm^{-2} the measured O:Ca Kα peak area ratio approached a steady state value of approximately 1.2:1, where complete conversion of $CaCO_3$ to CaO would be

expected to give 1:1. This small difference in measured and expected ratios was most likely due to the assumptions made when calculating the k-factor for quantification of the O:Ca atom ratio, although it is also possible that it is due to incomplete conversion of $CaCO_3$ to CaO, or that CO_2 remains trapped in the particles in closed pores/voids.

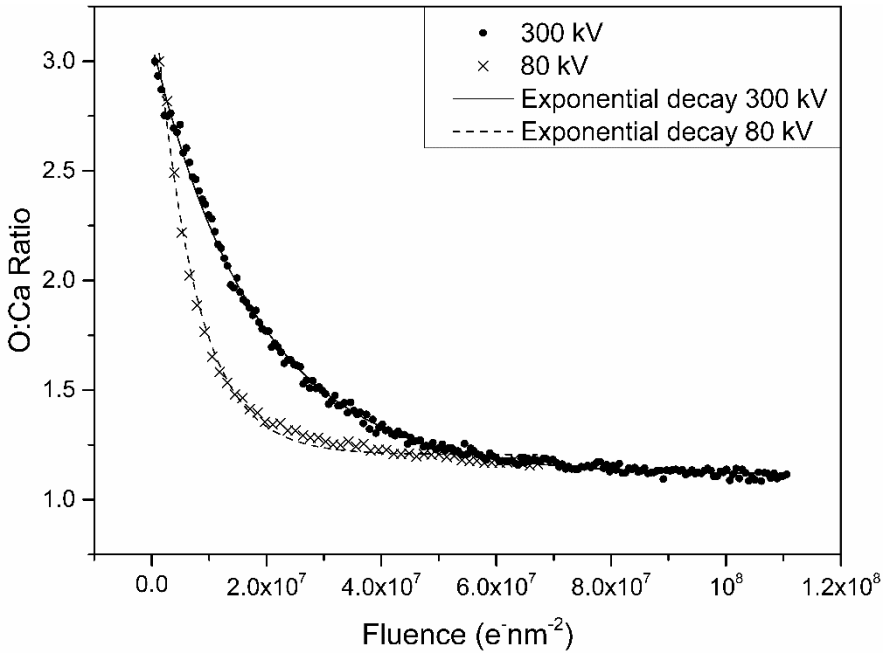

Figure 5 - Influence of irradiation voltage on the reduction of O:Ca ratio determined by EDX spectroscopy in CTEM, with exponential fits to the decay curves also shown. Electron fluxes were $3.5x10^4$ $e^-nm^{-2}s^{-1}$ for both 80 and 300 kV.

The decay of O:Ca *Kα* peak area ratio follows an exponential form, with the characteristic or critical fluence for the reduction of O:Ca atomic ratio to 1/e giving an indication of the rate of mass loss. The characteristic fluence threshold for mass loss at 300 kV was $1.9x10^7$ e^-nm^{-2}, whereas at 80 kV this was reduced to $7.9x10^6$ e^-nm^{-2}. Rodriguez-Navarro et al., (2009) stated that the de-excitation process resulting in bond fission is the rate limiting step here because the resulting transformation of calcite to calcium oxide would leave sufficient pores and voids for rapid out-diffusion of CO_2. The existence of nanoporosity was supported by the bright field CTEM imaging already presented here (Figure 1, Figure 3 and Figure 4).

At fluences greater than 10^8 e^-nm^{-2} calcium carbonate was essentially transformed to polycrystalline calcium oxide. To make use of EDX information without significant compositional degradation, a suitably low fluence must be used, however this will lead to poor X-ray counts. Figure 6 displays the X-ray counts for individual calcite nanoparticles, irradiated

for the same accumulated fluence (of $1x10^6$ e^-nm^{-2} at a flux of $3.4x10^4$ $e^-nm^{-2}s^{-1}$) at 80 kV and 300 kV in order to evaluate whether the increase in X-ray counts provided by 80 kV operation outweighs the increase in damage.

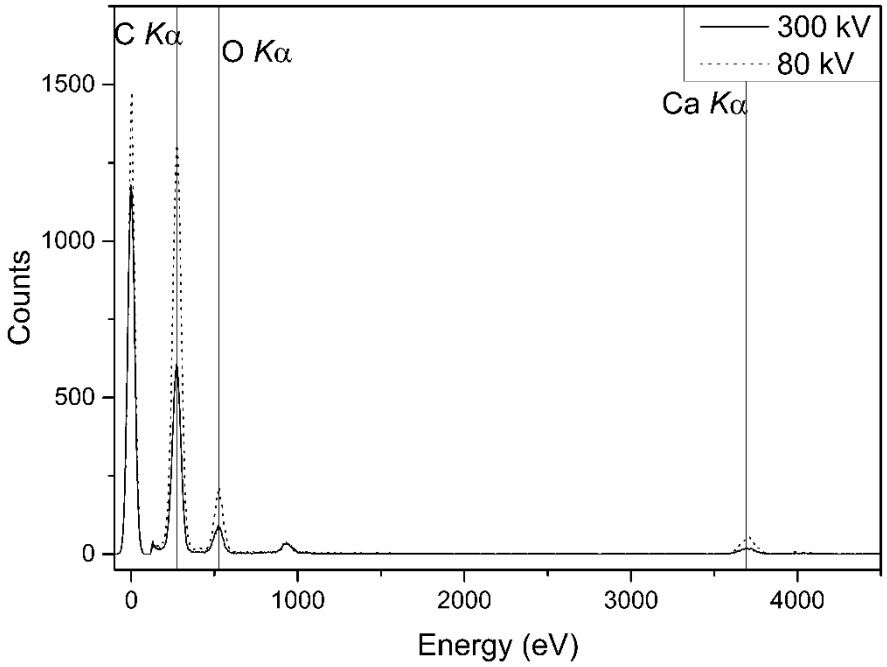

Figure 6 – Averaged CTEM EDX spectra for individual calcite nanoparticles irradiated at 300 kV and 80 kV under the same accumulated fluence of $1x10^6$ e^-nm^{-2} at a flux of $3.4x10^4$ $e^-nm^{-2}s^{-1}$.

For the same total accumulated fluence, a single EDX spectrum acquired at 80 kV did indeed show an increased number of total counts and count rate over 300 kV operation (Figure 6). However this increase in signal was almost exactly offset by the reduction in specimen lifetime: at 80 kV (relative to 300 kV) the average peak areas for Ca Kα and O Kα increased by a factor of 2.7 and 2.3 respectively, whilst the characteristic fluence for compositional change reduced by a factor of 2.4. At 300 kV, the same increase in X-ray counts could be achieved by simply collecting X-rays for longer whilst reaching the same extent of specimen damage as observed at 80 kV. This is well known (e.g. Egerton, 2014) and arises since the dose (the energy) deposited in a specimen (of identical thickness) will be the same. This, coupled with the potential reduction in damage onset for phase contrast CTEM imaging (Figure 3 and Figure 4) indicated that there was no obvious benefit to the irradiation lifespan of calcium carbonate at 80 kV operation.

3.3 Comparing CTEM and STEM irradiation at 300 kV

Under 300 kV STEM irradiation, crystalline CaO was not visible in the FFT of the PC-STEM image, even up to an accumulated fluence of 1.9×10^8 $e^- nm^{-2}$ (Figure 7). Despite the obvious formation of pores or bubbles, changes in projected shape of the particles and clear hydrocarbon contamination build up, the general form of the imaged calcite lattice is retained across these fluences. This possibly suggests that STEM may be a better choice for prolonged imaging of calcium carbonate based materials, at least where hydrocarbon contamination is present. It was notable that no crystalline CaO is observed under STEM irradiation, despite the change in shape of the particle and the clear pore formation (Figure 7A-C). This would suggest that the progression of radiolysis is limited by the hydrocarbon coating and that calcium oxide crystallization was completely inhibited (one presumes some amorphous CaO must have formed as mobile pores or gas bubbles were readily visible under the contamination layer, and CTEM EDX results show that significant mass loss could have occurred by this fluence with the O:Ca atomic ratio reduced to ~1.5:1).

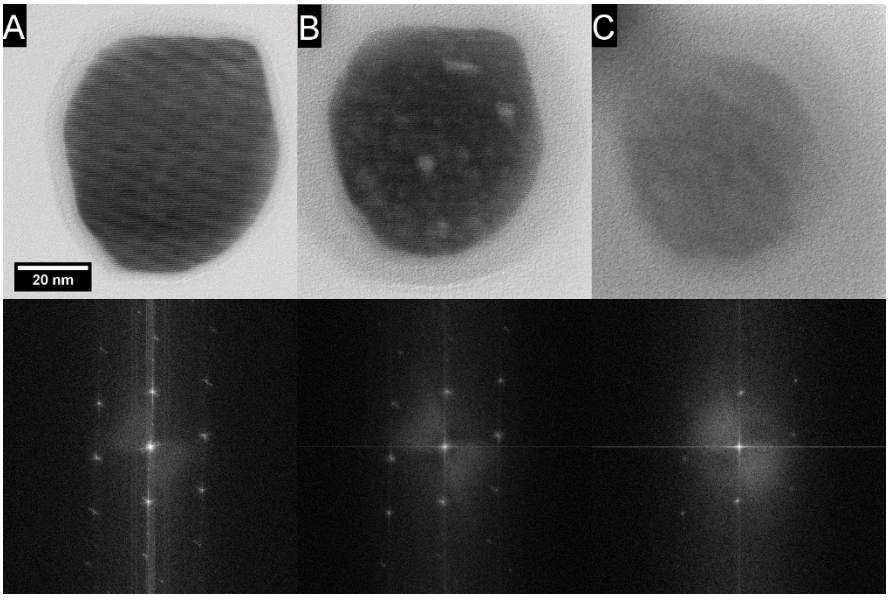

Figure 7 - PC-STEM images and FFTs (indicating the $[4\bar{4}1]$ zone axis of the calcite nanoparticle) at different accumulated fluences: A 1.2×10^6; B – 2.7×10^7 and C - 1.9×10^8 $e^- nm^{-2}$. 20 nm scale bar.

The formation of a contamination layer may be reducing the mobility of damage products by acting as a diffusion barrier, reducing the extent of mass loss, or acting to enhance the sample

conductivity and hence charge build up in the specimen in a similar manner to intentionally deposited carbon coatings. However, it is not clear at this stage what is actually inhibiting the nucleation of CaO. Nonetheless, STEM imaging confirms that calcite degradation begins with a reduction in crystallinity. Eliminating or minimising the presence of hydrocarbon contamination should then reveal whether irradiation effects in STEM are similar to those already noted in CTEM.

3.4 In situ bake-out

Removal of hydrocarbon contamination was achieved by heating the sample in an in-situ TEM heating holder at 75ºC for 16 hours in the microscope column in order to encourage thermal desorption of the contaminants. Prior to heat treatment, hydrocarbon contamination accumulated rapidly around particles, reaching an average of 15 nm thickness after 10 STEM scans, (Figure 9). Following in-situ heat treatment for 16 hours, little or no contamination was detected after 10 STEM scans and a significant reduction in contamination was seen even after as little as 10 minutes of in-situ heating at the same temperature (Figure 9).

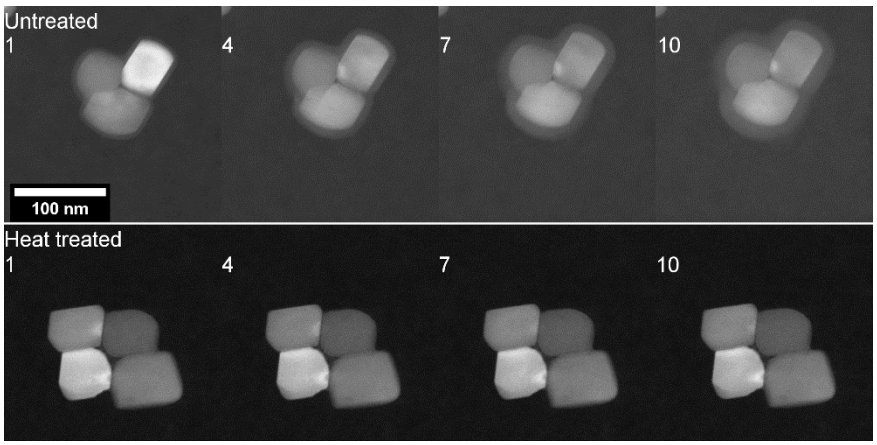

Figure 8 – ADF-STEM images of calcite particles after 1, 4, 7 and 10 scans. Top row - prior to in situ heat treatment. Bottom row - after 16 hours of in-situ heat treatment at 75ºC, sample cooled to 25ºC before imaging. 100 nm scale bar.

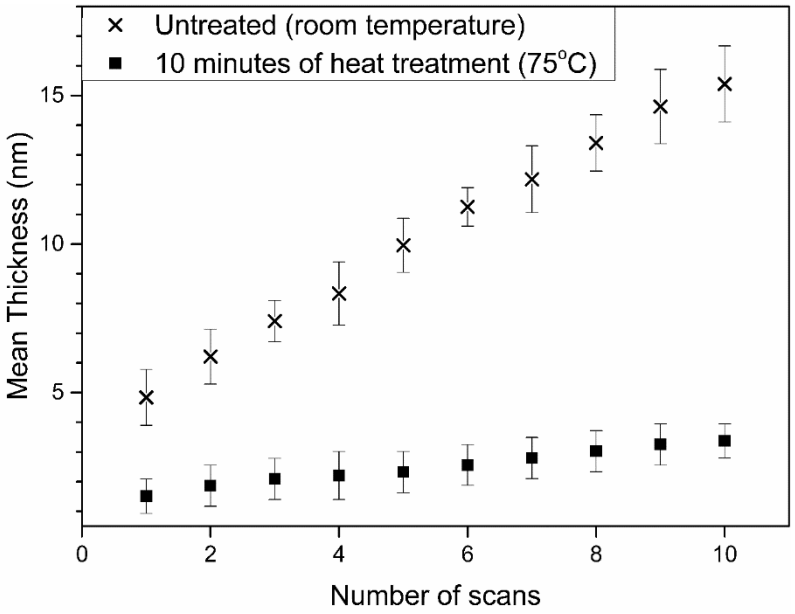

Figure 9 – Observed thickness of the hydrocarbon contamination layer, measured by ADF STEM imaging, as a function of STEM scan number both at room temperature and following 10 minutes of in-situ heat treatment at 75 ºC. Error bars correspond to standard deviation from the measured mean.

The reduction of hydrocarbon contamination allowed for an investigation into the true electron beam sensitivity of calcite using 300 kV phase contrast STEM imaging. In STEM, without the presence of hydrocarbon contamination, calcite degraded at lower fluences than when contamination was present. On average, polycrystalline calcium oxide was seen in the FFT at 1.1×10^7 $e^- nm^{-2}$ (Figure 10c), however dark features were seen in the images before this (Figure 10b), with these features displaying crystallinity following further irradiation, and these are likely beam-induced defects within the calcite lattice. This represents a similar fluence for the onset of calcite degradation as that observed using 300 kV CTEM illumination using an ultrathin amorphous carbon film to support calcite particles (2.7×10^7 $e^- nm^{-2}$). A ~1-2 nm amorphous layer was seen around the calcite particles under CTEM irradiation (Figure 3),

suggesting that a small build-up of contamination was present, however this did not appear to grow with continuing irradiation.

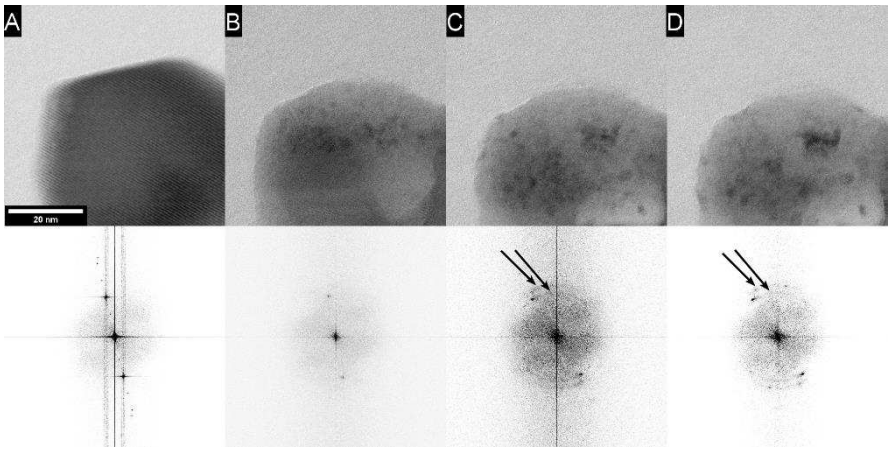

Figure 10 – 300 kV PC-STEM irradiation series and corresponding FFT processed with "reveal weak reflections" setting of Difftools plugin in GMS 3.11. A = 1.5x10^{6}, B = 6x10^{6}, C = 1.1x10^{7}, D = 1.5x10^{7} e^{-}nm^{-2}, on a calcite nanoparticle following in-situ heat treatment. Image A and B display calcite crystallinity, polycrystalline calcium oxide is first detected in the FFT at 1.1x10^{7} e-nm^{-2} indicated by the arrows in image C and D, 20 nm scale bar.

Repeated STEM scans (and associated FFTs) showed that cleaned calcite particles lost crystallinity before the nucleation of crystalline calcium oxide was detected, unlike in CTEM imaging. This was apparent in the FFTs in Figure 10, as the intensity of the amorphous scattering in the FFT increased whilst the crystalline calcite spot intensity concurrently reduced (Figure 10). In addition the faceting of the irradiated particle degraded with increasing irradiation, with the original crystalline facets roughening and possibly rearranging into "nanofacets" before the particle becomes fully amorphous (for example see the projected surface facet at the top of the particle in the image series of Figure 10). Taken together these results suggested the presence of an amorphous intermediate of either calcium carbonate, calcium oxide or both during the damage process, prior to the eventual crystallisation of calcium oxide.

4 Discussion

300 kV operation has been shown to have benefits over 80 kV for phase contrast imaging of calcite nanoparticles by CTEM (Figure 3 and Figure 4), this was due to the reduction in

inelastic cross section giving an increase in the inelastic mean free path. Whilst this was beneficial for imaging, the reduced inelastic interaction at 300 kV means that there are fewer counts for EDX and EELS (Figure 6). The reduction in EDX signal was similar in magnitude to the increase in calcite specimen lifetime at 300 kV (Figure 5 and Figure 6), so the reduced sensitivity was offset by the increase in collection times required to achieve the same signal to noise level in EDX data (as discussed by Egerton, (2014)).

Whilst increasing the accelerating voltage from 80 kV to 300 kV increased the critical fluence for the degradation of calcite, it reduces the image contrast proportionally, and thus one would expect the dose limited resolution to remain unchanged (Egerton, 2014). However, the performance of the imaging detector is also a factor and the image contrast is affected by the detective quantum efficiency (DQE) and modulation transfer function (MTF). Thus, the imaging mode may have implications for the dose limited resolution. Photomultiplier based STEM detectors can be considered point detectors as they collect signals in a serial manner, and will display an improved MTF at standard collection conditions, as compared to a pixelated detector used for CTEM imaging (Sader et al., 2010). If STEM point detectors can be optimised for pulse readout, the MTF of STEM can be enhanced, improving the contrast and thus improving the dose limited resolution when compared to a CTEM CCD or CMOS camera with the same detective quantum efficiency (DQE) (Jones and Downing, 2018).

STEM offers an improved irradiation lifetime over CTEM for radiation sensitive materials displaying a non-linear/inverse dose rate dependence i.e. increasing fluence rate does not cause a linear increase in damage rate, typically such damage processes are diffusion limited. In the case of calcite, which displays a linear relationship between fluence rate and damage rate (Hooley et al., 2017), the extent of damage was directly proportional to the accumulated fluence and so it would be expected that there would be no inherent benefit to the use of STEM over CTEM to avoid damage.

STEM operation does however offer advantages for calcium carbonate based materials in terms of fluence efficiency for a fixed damage threshold including “off specimen” focussing and fine probe alignment using the Ronchigram on the support film to reduce pre-

irradiation of the region of interest, and simultaneous phase contrast and elastic annular dark field imaging to identify regions of interest. We also show here that hydrocarbon contamination generated by fine probe scanning appears to extend the damage thresholds in calcite nanoparticles (Figure 7 and Figure 10), where a similar effect has been noted in the sheet silicate mineral biotite by Ward et al., (2013). There are several potential reasons why contamination extends the lifetime of calcite under irradiation: the use of an intentionally deposited coating has been demonstrated to reduce knock-on and radiolysis induced sputtering damage in multiple reports (Egerton, 2013; Egerton et al., 2006; Fryer, 1984; Muller and Silcox, 1995; Ward et al., 2013). Fryer and Holland, (1984) has suggested that for radiolysis, carbon coatings may aid in the recombination process of molecular fragments, as the fragments are retained in the original proximity by the carbon coat. By extension this mechanism would also reduce the mobility of damage products, in turn reducing the rate of mass loss for fragments which do not recombine. It is also likely that the contamination layer itself may aid in the dissipation of electrical charge and heat. Whilst we believe that irradiation induced hydrocarbon contamination has benefits, a balance must be struck between extending the lifespan of beam sensitive materials, and the negative impacts of contamination build-up; including the reduction in image contrast, reduced X-ray counts due to absorption in the contamination layer and the interference of the signal from adventitious carbon in electron energy loss spectra.

In CTEM, phase contrast imaging has a high electron collection efficiency, however when imaging weak phase objects it is often challenging to achieve optimum focus visually under low dose conditions. Phase contrast STEM offers relatively poor collection efficiency of electrons when reciprocity conditions are used, but focussing is simplified using the Ronchigram of the support film. Also, by relaxing reciprocity conditions, it is possible to increase the collection efficiency of electrons, whilst forming phase contrast images (Rose, 1974). Previous work by Sader et al., (2010) has shown it is possible to acquire phase contrast STEM images of adequate contrast and signal to noise ratio, whilst maintaining moderate collection efficiency by setting the bright field detector to be approximately half the size of the

zero order STEM disc as originally suggested by Rose, (1974). The phase contrast STEM conditions used here followed those reported by Sader et al., (2010) and therefore provided approximately 25% collection efficiency. Whilst this is relatively low compared to CTEM, it was counteracted by the improved ease of focus using the Ronchigram, and retained the potential for simultaneous collection of multiple imaging and elemental signals.

Collection efficiency and signal to noise ratio can further be improved through recent developments in STEM integrated differential phase contrast (iDPC) using a segmented detector as well as focussed probe ptychography with a pixelated detector, where the signal to noise ratio is able to exceed CTEM phase contrast images (Sagawa et al., 2018; Yücelen et al., 2018). Both iDPC and ptychography have shown promise for the study of beam sensitive materials and light element containing materials at atomic resolution due to the efficiency of electron collection at low probe currents.

Fluence-efficient imaging using STEM with a low probe current is a powerful tool for the study of radiation sensitive materials previously precluded or severely limited by CTEM investigation. Especially where both phase contrast and elastic annular dark field imaging can provide insights into structure and crystallinity. An example of this is the study of calcium carbonate based industrial fuel detergents, generally considered to be amorphous at sub 10 nm particles sizes (Hudson et al., 2006). In such cases, diffraction contrast generated with STEM ADF imaging aids in the identification of potentially crystalline regions and phase contrast can provide structural or polymorph information at high resolution. Electron collection conditions can easily be adapted for aberration-corrected or uncorrected STEM systems to either maximise the amount of phase contrast available, or maximise the collection efficiency, whichever is most beneficial in that instance.

5 Conclusions

High voltage STEM has great potential for the analysis of materials sensitive to radiolysis, offering opportunity for low fluence, high resolution imaging under suitable collection conditions. For the case of calcite nanoparticles, 300 kV STEM offers significant benefits over

CTEM, however only where contamination is present, increasing the fluence threshold for the detection of irradiation induced faults in the calcite lattice from $2.7x10^7$ e^-nm^{-2} for 300 kV CTEM to over $1.8x10^8$ e^-nm^{-2} for 300 kV STEM. It was found that 80 kV operation offered no benefits for phase contrast imaging of calcite nanoparticles when compared to 300 kV operation, nor any benefits for EDX spectroscopy, where the characteristic fluence for mass loss reduced from $1.9x10^7$ e^-nm^{-2} for 300 kV to $7.9x10^6$ e^-nm^{-2} for 80 kV operation.

For fluence-efficient imaging of calcite nanoparticles, the optimal conditions suggested by this study include 300 kV STEM with simultaneous bright field phase contrast, elastic annular dark field imaging and this could routinely be coupled with EDX for compositional insights.

Acknowledgements

RH acknowledges a studentship funded through the EPSRC CDT in Complex Particulate Products and Processes (cP^3-CDT) and acknowledges co-funding from Thermo-Fisher Scientific (formerly FEI Co). RH also would like to thank Prof. Fiona Meldrum and Dr. Alex Kulak for assistance in the synthesis of the calcite nanoparticles.
The authors would like to acknowledge the LEMAS microscopy facility for access to instruments and for technical support. Funding for the FEI Titan^3 Themis microscope was provided through EPSRC grant EP/M028143/1.

Declaration of interests: none

References

Cazaux, J., 1995. Correlations between ionization radiation damage and charging effects in transmission electron microscopy. Ultramicroscopy 60, 411-425.http://dx.doi.org/10.1016/0304-3991(95)00077-1

Chen, C.L., Arakawa, K., Mori, H., 2010. Effect of Pt on the electron-irradiation-induced decomposition of sapphire. Scripta Materialia 63, 355-358.http://dx.doi.org/10.1016/j.scriptamat.2010.04.007

Egerton, R.F., 2012. Mechanisms of radiation damage in beam-sensitive specimens, for TEM accelerating voltages between 10 and 300 kV. Microscopy research and technique 75, 1550-1556.http://dx.doi.org/10.1002/jemt.22099

Egerton, R.F., 2013. Control of radiation damage in the TEM. Ultramicroscopy 127, 100-108.http://dx.doi.org/10.1016/j.ultramic.2012.07.006

Egerton, R.F., 2014. Choice of operating voltage for a transmission electron microscope. Ultramicroscopy 145, 85-93.http://dx.doi.org/10.1016/j.ultramic.2013.10.019

Egerton, R.F., Li, P., Malac, M., 2004. Radiation damage in the TEM and SEM. Micron 35, 399-409.http://dx.doi.org/10.1016/j.micron.2004.02.003

Egerton, R.F., Wang, F., Crozier, P.A., 2006. Beam-Induced Damage to Thin Specimens in an Intense Electron Probe. Microscopy and Microanalysis 12, 65-71.http://dx.doi.org/10.1017/S1431927606060065

Fryer, J.R., 1984. Radiation damage in organic crystalline films. Ultramicroscopy 14, 227-236.http://doi.org/10.1016/0304-3991(84)90091-3

Fryer, J.R., Holland, F., 1984. High Resolution Electron Microscopy of Molecular Crystals. III. Radiation Processes at Room Temperature. Proceedings of the Royal Society of London. A. Mathematical and Physical Sciences 393, 353.http://dx.doi.org/10.1098/rspa.1984.0062

Golla-Schindler, U., Benner, G., Orchowski, A., Kaiser, U., 2014. In situ observation of electron beam-induced phase transformation of CaCO3 to CaO via ELNES at low electron beam energies. Microscopy and microanalysis : the official journal of Microscopy Society of America, Microbeam Analysis Society, Microscopical Society of Canada 20, 715-722.http://dx.doi.org/10.1017/S1431927614000464

Hari, B., Ding, X., Guo, Y., Deng, Y., Wang, C., Li, M., Wang, Z., 2006. Multigram scale synthesis and characterization of monodispersed cubic calcium carbonate nanoparticles. Materials Letters 60, 1515-1518.http://dx.doi.org/10.1016/j.matlet.2005.11.062

Hills, A.W.D., 1968. The mechanism of the thermal decomposition of calcium carbonate. Chemical Engineering Science 23, 297-320.http://doi.org/10.1016/0009-2509(68)87002-2

Hirsch, P., Kassens, M., Puttmann, M. & Reimer, L. 1994. Contamination in a scanning electron microscope and the influence of specimen cooling. Scanning, 16**,** 101-110.

Hoffmann, R., Wochnik, A.S., Betzler, S.B., Matich, S., Griesshaber, E., Schmahl, W.W., Scheu, C., 2014. TEM preparation methods and influence of radiation damage on the beam sensitive CaCO3 shell of Emiliania huxleyi. Micron 62, 28-36.http://dx.doi.org/10.1016/j.micron.2014.03.004

Hooley, R.W.M., Brown, A.P., Kulak, A.N., Meldrum, F.C., Brydson, R.M.D., 2017. A Quantitative Evaluation of Electron Beam Sensitivity in Calcite Nanoparticles. Journal of Physics: Conference Series 902, 012005.http://dx.doi.org/10.1088/1742-6596/902/1/012005

Hudson, L.K., Eastoe, J., Dowding, P.J., 2006. Nanotechnology in action: Overbased nanodetergents as lubricant oil additives. Advances in Colloid and Interface Science 123–126, 425-431.http://dx.doi.org/10.1016/j.cis.2006.05.003

Jacob, D.E., Wirth, R., Soldati, A.L., Wehrmeister, U., Schreiber, A., 2011. Amorphous calcium carbonate in the shells of adult Unionoida. Journal of Structural Biology 173, 241-249.http://dx.doi.org/10.1016/j.jsb.2010.09.011

Jones, L., Downing, C., 2018. The MTF & DQE of Annular Dark Field STEM: Implications for Low-dose Imaging and Compressed Sensing. Microscopy and Microanalysis 24, 478-479.http://dx.doi.org/10.1017/S143192761800288X

Kabalah-Amitai, L., Mayzel, B., Kauffmann, Y., Fitch, A.N., Bloch, L., Gilbert, P.U.P.A., Pokroy, B., 2013. Vaterite Crystals Contain Two Interspersed Crystal Structures. Science 340, 454-457.http://dx.doi.org/10.1126/science.1232139

Kovarik, L., Stevens, A., Liyu, A., Browning, N.D., 2016. Implementing an accurate and rapid sparse sampling approach for low-dose atomic resolution STEM imaging. Applied Physics Letters 109, 164102.http://dx.doi.org/10.1063/1.4965720

Mansot, J.L., Hallouis, M., Martin, J.M., 1993. Colloidal antiwear additives 1. Structural study of overbased calcium alkylbenzene sulfonate micelles. Colloids and Surfaces A: Physicochemical and Engineering Aspects 71, 123-134.http://dx.doi.org/10.1016/0927-7757(93)80336-D

Mitchell, D.R.G., 2008. DiffTools: Electron diffraction software tools for DigitalMicrograph™. Microscopy research and technique 71, 588-593.http://dx.doi.org/10.1002/jemt.20591

Muller, D.A., Silcox, J., 1995. Radiation damage of Ni3Al by 100 keV electrons. Philosophical Magazine A 71, 1375-1387.http://dx.doi.org/10.1080/01418619508244380

Murooka, Y., Walls, M., 1991. Beam damage in an anisotropic material (CaCO3) in STEM. Institue of physics, conference series 119, 121-124

Nielsen, M.H., Lee, J.R.I., Hu, Q., Yong-Jin Han, T., De Yoreo, J.J., 2012. Structural evolution, formation pathways and energetic controls during template-directed nucleation of CaCO3. Faraday Discussions 159, 105-121.http://dx.doi.org/10.1039/C2FD20050C

Rae Cho, K., Kim, Y.-Y., Yang, P., Cai, W., Pan, H., Kulak, A.N., Lau, J.L., Kulshreshtha, P., Armes, S.P., Meldrum, F.C., De Yoreo, J.J., 2016. Direct observation of mineral-organic composite formation reveals occlusion mechanism. Nat Commun 7.http://dx.doi.org/10.1038/ncomms10187

Ritchie, N.W.M., 2011. Getting Started with NIST DTSA-II. Microscopy Today 19, 26-31.10.1017/S155192951000132X

Rodriguez-Navarro, C., Burgos Cara, A., Elert, K., Putnis, C.V., Ruiz-Agudo, E., 2016. Direct Nanoscale Imaging Reveals the Growth of Calcite Crystals via Amorphous Nanoparticles. Crystal Growth & Design 16, 1850-1860.http://dx.doi.org/10.1021/acs.cgd.5b01180

Rodriguez-Navarro, C., Ruiz-Agudo, E., Luque, A., Rodriguez-Navarro, A.B., Ortega-Huertas, M., 2009. Thermal decomposition of calcite: Mechanisms of formation and textural evolution of CaO nanocrystals. American Mineralogist 94, 578-593.http://dx.doi.org/10.2138/am.2009.3021

Rose, H., 1974. Phase Contrast in Scanning Transmission Electron Microscopy. OPTIK 39, 416-436

Sader, K., Brown, A., Brydson, R., Bleloch, A., 2010. Quantitative analysis of image contrast in phase contrast STEM for low dose imaging. Ultramicroscopy 110, 1324-1331.http://doi.org/10.1016/j.ultramic.2010.06.008

Sagawa, R., Hashiguchi, H., Kondo, Y., 2018. Low Dose Ptychographic STEM Observation Using Fast Pixelated Detector. Microscopy 67, i27-i27.http://dx.doi.org/10.1093/jmicro/dfy080

Smith, M., 1986. Silver Coating Inhibits Electron Microprobe Beam Damage of Carbonates. Journal of Sedimentary Petrology Research 56, 560-561

Srot, V., Wegst, U.G.K., Salzberger, U., Koch, C.T., Hahn, K., Kopold, P., van Aken, P.A., 2013. Microstructure, chemistry, and electronic structure of natural hybrid composites in abalone shell. Micron 48, 54-64.http://dx.doi.org/10.1016/j.micron.2013.02.010

Towe, K.M., 1978. Ultrastructure of calcite decomposition in vacuo. Nature 274, 239.http://dx.doi.org/10.1038/274239a0

Walls, M., Tence, M., 1989. EELS study of beam induced decomposition of calcite in the STEM. IOP Conference Series EMAG89 98, 4

Ward, M.B., Kapitulčinová, D., Brown, A.P., Heard, P.J., Cherns, D., Cockell, C.S., Hallam, K.R., Ragnarsdóttir, K.V., 2013. Investigating the role of microbes in mineral weathering: Nanometre-scale characterisation of the cell–mineral interface using FIB and TEM. Micron 47, 10-17.http://dx.doi.org/10.1016/j.micron.2012.12.006

Yücelen, E., Lazić, I., Bosch, E.G.T., 2018. Phase contrast scanning transmission electron microscopy imaging of light and heavy atoms at the limit of contrast and resolution. Scientific reports 8, 2676.http://dx.doi.org/10.1038/s41598-018-20377-2